Bottom Boundary Mixing: The Role of Near-Sediment Density Stratification

A. Wüest and M. Gloor

Abstract

The turbulent dynamics and stratification of bottom boundary layers, as well as the net diapycnal buoyancy flux in the deep water, have been observed to vary strongly among lakes. The most relevant parameters governing the different regimes are the bottom current stress and the rate of release of dissolved solids from the sediment. The ratio of boundary-induced mixing to the density flux associated with the flux of ions from the sediment determines whether the bottom boundary layer is extremely stably stratified or well-mixed. The aim of this contribution is (1) to demonstrate these two boundary phenomena, (2) to give a physical criterion for assessing the two mixing regimes, (3) to present a potential model to quantify the boundary-induced buoyancy flux and the basin-wide diapycnal diffusivity, and (4) to test the model with data from two representative lakes with significantly different deep-water mixing characteristics.

The Stratification of the Bottom Boundary in Lakes

Limnologists often observe a distinctly different vertical stratification of water properties within the region directly above the sediment of lakes. Even though it is evident that this fact has implications for the ecology of the entire aquatic system, little attention has been paid so far to the detailed physical mechanisms within lacustrine bottom boundaries. Therefore, compared to the ocean, where the role of the bottom boundaries for basin-wide diapycnal mixing and transport has frequently been recognized and investigated (Wunsch, 1970; Armi, 1978; Garrett, 1979; Phillips et al., 1986; Ivey, 1987; Thorpe, 1988; Garrett, 1990; Toole et al., 1994), the number of studies in lakes is rather small (Imberger and Patterson, 1990; Imboden and Wüest, 1995).

In the first part of the paper we present data sets of currents and stratification from the bottom boundary of two lakes which are subjected to distinctly different external forcing and hence show drastically different deep-water mixing characteristics. The bottom boundary layer is considered here as the zone above the sediment which is predominantly affected by the stress due to bottom friction. The first example is from Alpnachersee (Figure 1), which is representative for lakes in which the bottom boundary layer is mostly

Physical Processes in Lakes and Oceans
Coastal and Estuarine Studies Volume 54, Pages 485-502

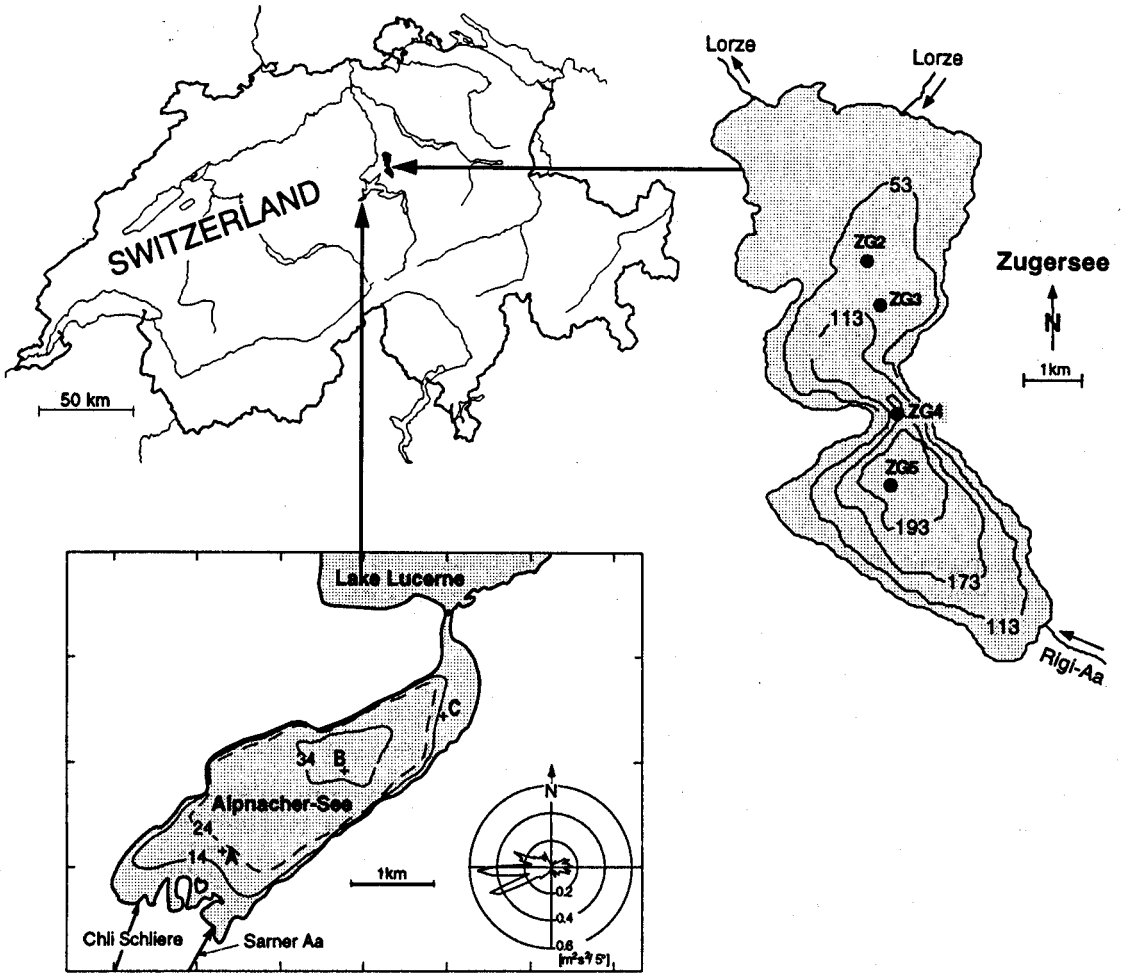

Figure 1. Location of the two Swiss lakes Alpnachersee and Zugersee. Alpnachersee is shallow (maximum depth 34 m) and small (surface area 4.8 km^2, volume: 0.1 km^3). It is exposed to a diel wind regime during summer (see inset) and is mesotrophic with respect to primary productivity. In contrast, Zugersee is a deep (maximum depth 198 m), medium-sized (surface area 38.3 km^2, volume: 3.2 km^3) lake which is sheltered from the prevailing Westerlies, and is highly productive. Depth contours are labelled in m. The marked positions refer to sampling stations mentioned in the text and in Figures 2 and 3.

of the well-mixed type, the second is from Zugersee (Figure 1), an example of a lake showing very strong near-sediment density stratification.

In the second part, we discuss the physical characteristics of the two boundary layers with extremely different stratification. Finally, we evaluate the relevance of bottom boundary stratification for the basin-wide diapycnal fluxes by presenting and applying a boundary mixing model. As the results of the model are consistent with basin-wide tracer diffusivity observations, we conclude that the model provides a reasonable description of the diapycnal fluxes in stratified enclosed water bodies with simple shapes.

(a) The "Alpnachersee case": Internal Seiches as the Source of Bottom Boundary Mixing

Alpnachersee is a small and relatively shallow (max. depth = 34 m) side-basin of Lake Lucerne (see morphometry in Figure 1). In summer, the mountain and valley breezes along the nearby mountains result in a predominantly diel wind that blows regularly parallel to

the major axis of the lake (Figure 1; for details see Münnich et al., 1992). Under such conditions, internal seiching and corresponding deep-water currents are excited in this lake (Gloor et al., 1994), as illustrated in Figure 2 for a two-month period during the summer of 1994.

In June and July 1994, the bottom boundary current oscillated with an amplitude of about 3-5 cms^{-1} and sporadically reached maximum speeds of up to 6-7 cms^{-1}. Power spectral analysis (Press et al., 1986) of the current and isotherm time series reveal that the two dominant periods (of about 8 and 24 hours: Gloor et al., 1994), correspond to the first vertical first horizontal and second vertical first horizontal seiche modes, schematically shown in Figure 3 and described mathematically by Münnich et al. (1992). For both modes, bottom currents along the major axis of the lake correlate well with the displacements of the hypolimnetic isotherms, as shown in detail by Gloor et al. (1994).

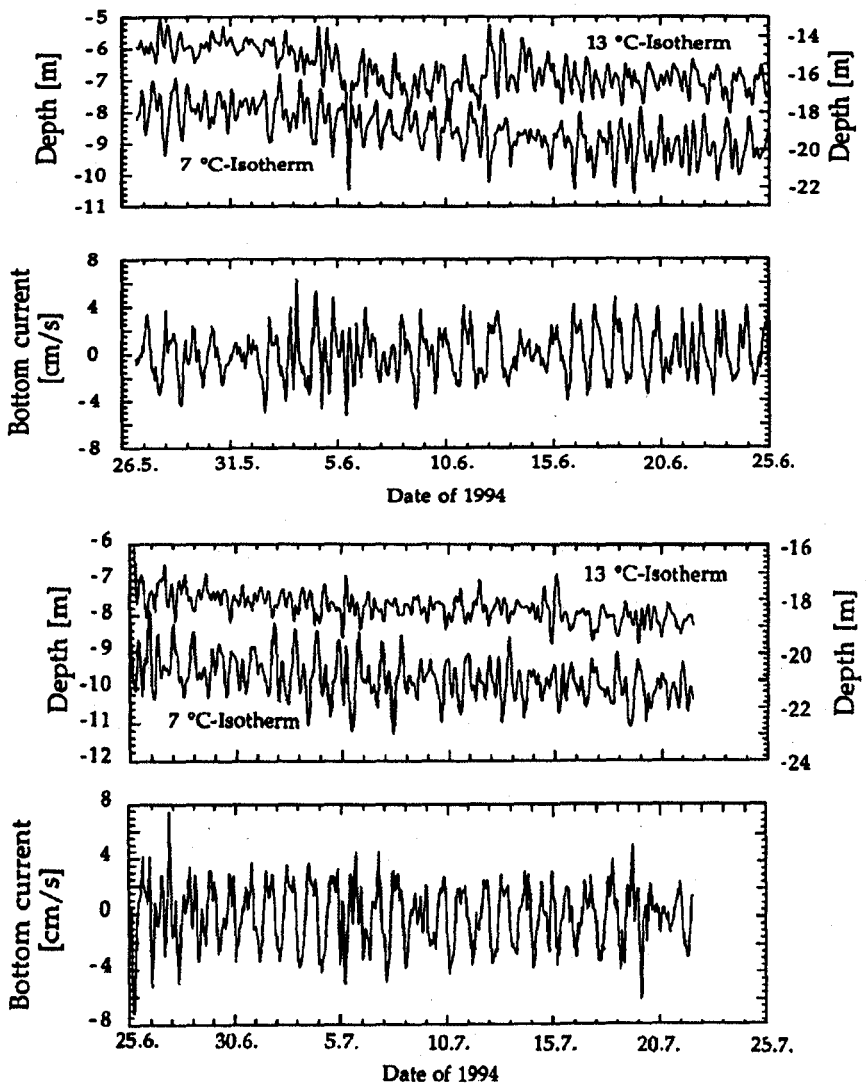

Figure 2. Upper panels: Time series of the depths of two selected isotherms at mooring A (Figure 1). The 7 °C and 13 °C isotherms refer to the right-hand and left-hand depth scales, respectively. The data, slightly filtered (time window: 1h), show the dominance of the strong second vertical seiche mode (Figure 3). Lower panels: Component of the bottom current along the major axis of Alpnachersee, measured at mooring B (Figure 1), 1.4 m above the sediment at the deepest part of the lake (positive values indicate current flowing towards ENE). Data from Gloor (1995).

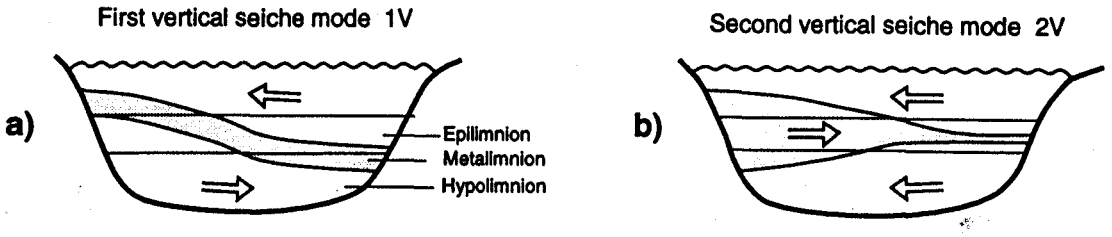

Figure 3. Schematic illustration of the vertical structure of the displacement of the first vertical (two-layer), and the second vertical (three-layer) seiche modes revealed in the data of Figure 2. The arrows indicate flow directions after maximum displacement of the layers.

a)

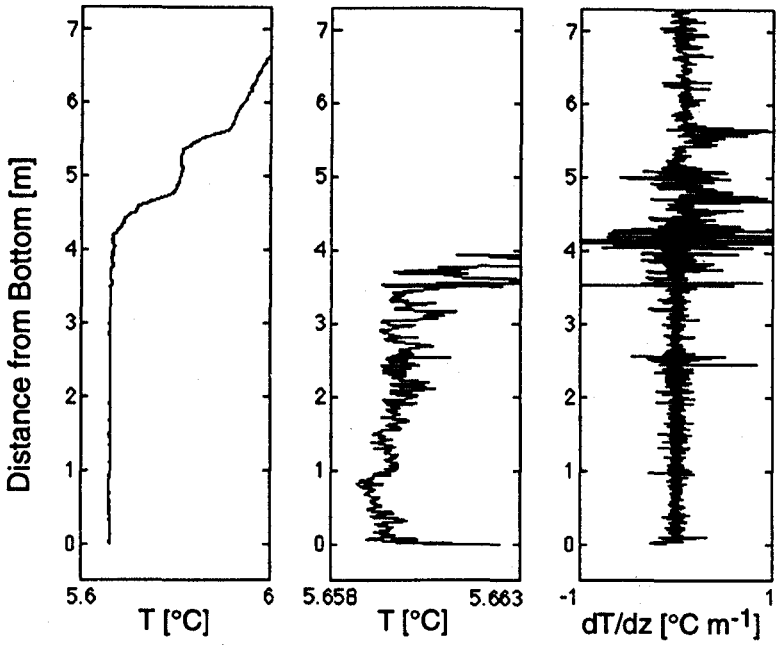

Figure 4a. An example of a temperature microstructure profile measured at mooring B (Figure 1) on June 2, 1994, down to a distance of about 8 cm above the sediment. In the well-mixed bottom layer of thickness $\delta_{mix} \approx 4.2$ m (left-hand panel) the temperature is homogeneous to within about 1 mK (middle panel). The double-sided gradient of the temperature microstructure indicates active mixing (right-hand panel).

The corresponding phases demonstrate that the whole hypolimnetic water body is excited by seiches of the first horizontal modes.

As an effect of the basin-wide hypolimnetic current field, the lower part of the bottom boundary is well-mixed (Figure 4a). The stability $N^2 = -g\rho^{-1}\,\partial\rho/\partial z$ (g = acceleration due to gravity; ρ = water density; z = vertical co-ordinate, positive upwards) dropped by more than an order of magnitude from $2\cdot10^{-5}$ s^{-2} in the overlying stratified water column to $7\cdot10^{-7}$ s^{-2} within the well-mixed layer. (The temporal average of $\approx 1.5\cdot10^{-6}$ s^{-2} is twice as large as this due to seiching motion as observed from within a Eulerian frame). Temperature microstructure measurements reveal that the layer is actively mixed by turbulence generated near the sediment (Figure 4a). This is not surprising, as the Richardson gradient number $Ri = N^2\,(\partial u/\partial z)^{-2}$ is approximately unity within the well-mixed layer if the shear is approximated by the law of the wall, i.e. $\partial u/\partial z = u_*(kz)^{-1}$ (where u_* is the friction velocity and $k = 0.41$ is the von Kàrmàn constant). Strong signals of temperature microstructure at the top of the well-mixed layer indicate entrainment from the thermally stratified

overlying water column. In the thermocline, double-sided signals, characteristic of active mixing, are only occasionally observed (as in Figure 4a).

For 300 temperature microstructure profiles taken along the main axis of the lake, the thickness δ_{mix} of the well-mixed layer was determined semi-automatically (and checked visually) by a gradient criterion for an abrupt change in the temperature profile. The thickness was observed to vary with the phase and intensity of the seiching motion and the depth of the lake bottom at the site. The frequency distribution of the occurrence of the mixed layer thicknesses (Figure 4b) shows that the arithmetic mean of the thickness of the well-mixed layer $\langle\delta_{mix}\rangle = \int \delta'_{mix} \cdot P(\delta'_{mix})\, d\delta'_{mix}$ was about 2.6 m in the deepest part and 0.6 m at mid-depth in Alpnachersee (where $P(\delta'_{mix})\, d\delta'_{mix}$ is the frequency of occurrence of the thickness δ'_{mix} to $\delta'_{mix} + d\delta'_{mix}$ of the well-mixed layer). Due to the seiching motion, averaging δ_{mix} at maximum depth underestimates the true thickness, which is maximally about 4 to 5 m (Figure 4a,b).

(b) The "Zugersee Case": Stratification by Dissolved Solids Emanating from the Sediment

A completely different density structure has been found in Zugersee, a medium-sized lake with a maximum depth of 198 m (see morphometry in Figure 1), characterized by high primary productivity and ineffective vertical mixing at large depths (Wehrli et al., 1994). Due to the correspondingly high gross sedimentation and mineralization rates of algal matter, significant quantities of dissolved solids (mainly HCO_3^- and Ca^{2+}) are released into the deep hypolimnion. Combined with the low wind exposure (the lake is sheltered from

b)

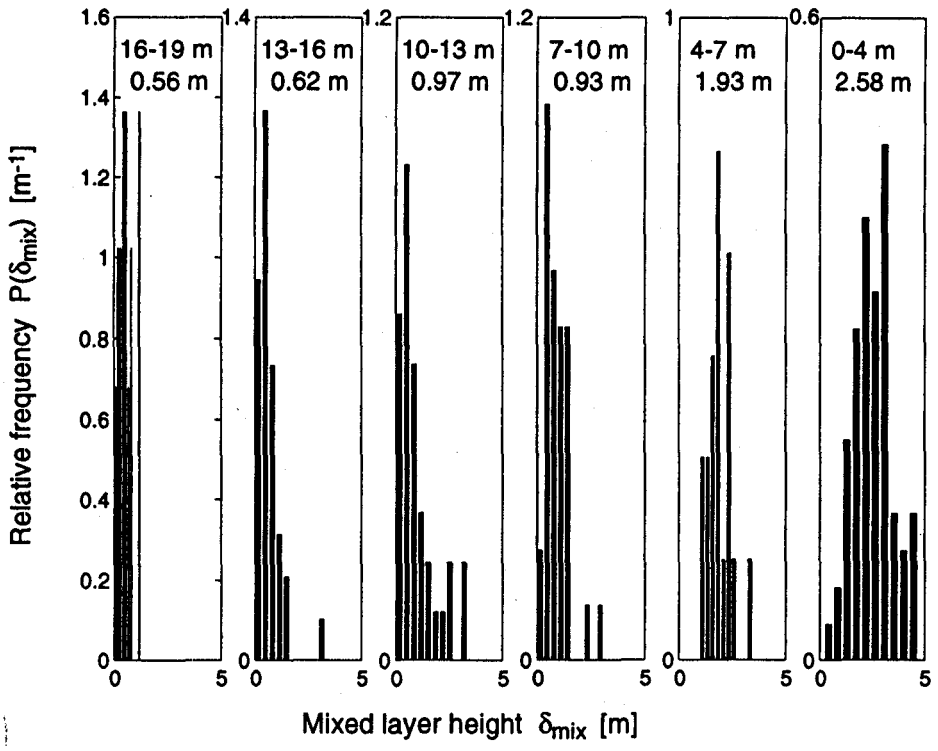

Figure 4b. Relative frequency of occurrence of the thickness δ_{mix} of well-mixed bottom layers such as that depicted in (a). The upper numbers indicate the height above maximum depth (i.e. 16-19 m) and the lower number represents the average mixed layer thickness found in that depth range (i.e. 0.56 m). Data from Gloor (1995).

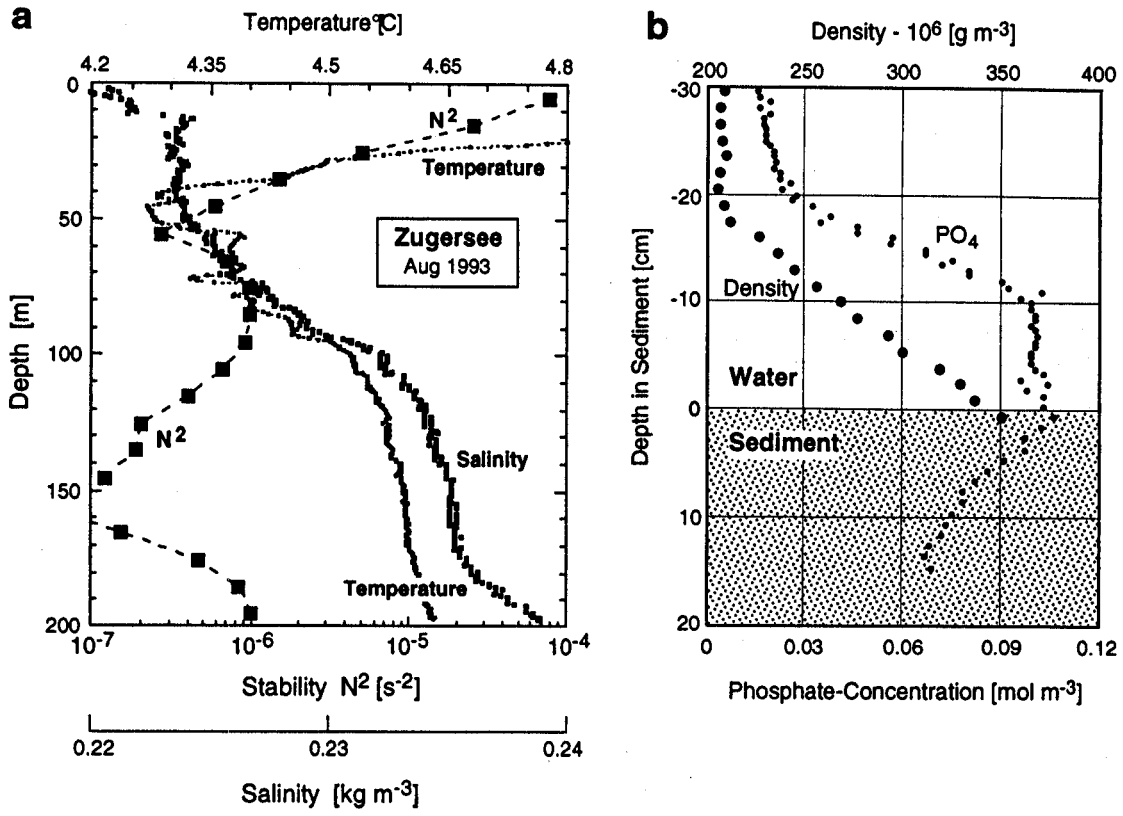

Figure 5. (a) Vertical profiles of temperature, salinity and stability N^2 (Position ZG5; Figure 1), measured in August 1993. The deep water of Zugersee, below about 80 m depth, is permanently biogenically density-stratified due to the release of dissolved solids from the sediment. (Structures above 80 m depth are remnants from mixing during the previous winter). The geothermal heat flux (≈ 0.1 Wm^{-2}; Finckh, 1981) is the cause of the inverse temperature gradient. The stabilizing effect of the dissolved solids is however several times greater than the destabilizing effect of the geothermal heat flux (Wehrli et al., 1995). Figure 5. (b) Profiles of density and PO_4 at the sediment interface at position ZG5 (Figure 1), the deepest part of Zugersee (note the vertical scale). The stability N^2 within the first 20 cm above the sediment is ≈ $8 \cdot 10^{-3}$ s^{-2}, which is extremely high compared to the open-water stability.

the prevailing Westerlies, and southerly winds are only sporadic: see Imboden et al., 1988), the mineralization-induced redissolution from the sediments has led to an accumulation of dissolved solids (Figure 5a), and consequently to a permanent biogenic density stratification in the deep water (Wehrli et al., 1995). The effect of salinity (defined as the mass of dissolved solids in g per kg of water) on the density stratification was determined following the procedure given by Wüest et al. (1996b), using molal volumes of the specific chemical composition of the lake water.

In the last few decades, vertical mixing during the cold winter period has not reached further than about 50 to 80 m depth, despite the increase in the temperature in the lower hypolimnion due to geothermal heating from the earth's interior (Figure 5a). The deep-water density stratification shows an interesting structure: the stability N^2 reaches a minimum of ≈10^{-7} s^{-2} at 160 m depth, but increases again to ≈10^{-6} s^{-2} towards the maximum depth (198 m). A microscopic view of the sediment-water interface reveals an even stronger gradient just above the sediment surface. Within an extremely stratified 20 cm thick near-sediment layer (Figure 5b), the stability N^2 jumps by several orders of

magnitude to $\approx 8 \cdot 10^{-3}$ s^{-2}. The density profile in Figure 5b was determined based on HCO_3^- and Ca^{2+} concentrations measured by the peeper technique (Brandl and Hanselmann, 1991) with a 1.5 cm vertical resolution.

Such strong gradients indicate that turbulent mixing above the sediment is being drastically reduced to nearly molecular level. This can be concluded by two arguments: (1) The time required to accumulate the measured ion concentration of HCO_3^- and Ca^{2+} within the 20 cm thick stratified near-sediment layer is comparable to the seasonal time scale. Given a rate of release of dissolved solids from the sediment of $F_{sed} \approx (2 \text{ to } 3) \cdot 10^{-6}$ $gm^{-2}s^{-1}$ (Wehrli et al., 1995) and the amount of ions (HCO_3^- and Ca^{2+}) contained within the 20 cm thick bottom layer shown in Figure 5b, a time scale of 2 months is obtained. (2) The molecular flux associated with the gradient of that layer is compatible (within a factor $\lesssim$ 2) to F_{sed}. This observation is also consistent with the phosphorus flux from the sediment and its accumulation shown in Figure 5b.

Having observed such strong stratification above the sediment, we were curious about the magnitude of the bottom current velocities in the deep hypolimnion. Measurements conducted at the deepest location during the period of low overall stratification in winter 1992-1993 revealed oscillating currents with typical amplitudes smaller than 2 cms^{-1} (Figure 6a,b). Unfortunately, during summer (the sampling time of the profile in Figure 5b), data collection at the deepest position failed. However, measurements near the mean lake depth during summer indicate that the current at the deepest location must have been even smaller (Figure 6c).

The Effect of the Release of Dissolved Solids on Mixing

As shown in the previous section, the near-sediment density gradients in Alpnachersee and Zugersee are completely different. In order to evaluate these differences we make use of the turbulent kinetic energy (TKE) balance. In non-stratified water, the production of TKE, driven by bottom friction, can be characterized by the scaling law (Dewey and Crawford, 1988)

$$\varepsilon = \frac{u_*^3}{k\,z} = \frac{C_{1m}^{3/2}}{k\,z}\,u_{1m}^3, \qquad [Wkg^{-1}] \qquad (1)$$

which quantifies dissipation ε as a function of the bottom velocity u_{1m} (1 m above bottom) and as a function of the distance z from the sediment ($u_* = C_{1m}^{1/2}\,u_{1m}$, and C_{1m} is the bottom drag coefficient). In turn, "negative" TKE is introduced by the buoyancy flux (local rate of change of potential energy) due to the flux of dissolved solids F_{sed} from the sediment. For $F_{sed} \approx 2.5 \cdot 10^{-6}$ gm^{-2} s^{-1}, the related buoyancy flux $J_b^{sed} = (g\beta/\rho) \cdot F_{sed} \approx 2 \cdot 10^{-11}$ Wkg^{-1} (β is the coefficient of haline contraction, with $\beta \approx 0.79$ $‰^{-1}$ for calcareous water: Chen and Millero, 1986; Wüest et al., 1996b). The Monin-Obukhov length scale

$$L_{MO} = \frac{u_*^3}{J_b^{sed}}, \qquad [m] \qquad (2)$$

the distance above the bottom where the production of turbulence due to the bottom current u_{1m} and its consumption due to the buoyancy flux J_b^{sed} are equal, provides a measure for the suppressing effect of the flux of dissolved solids (Figure 7). The comparison for Alpnachersee and Zugersee yields:

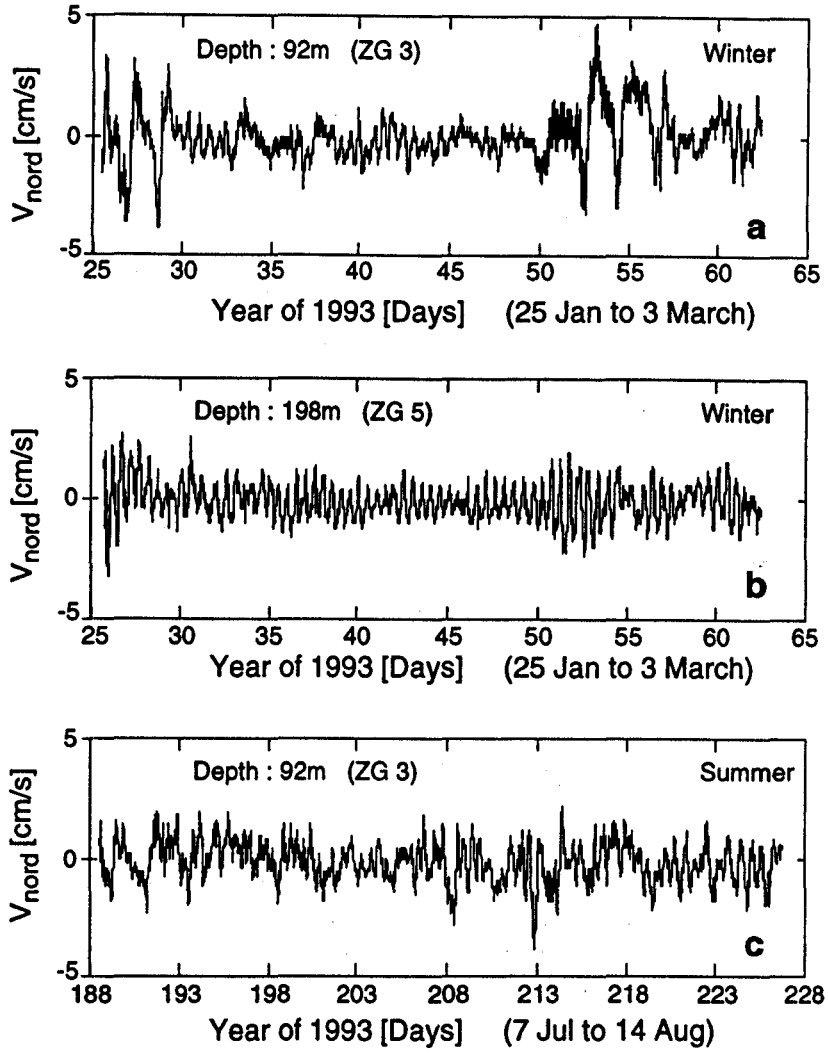

Figure 6. The component of the bottom current along the major axis of Zugersee during the winter considered in this paper (upper two panels) and the following summer period (lower panel). Measurements in the deepest part were carried out in the southern basin (position ZG5; Figure 1), whereas measurements near the mean depth were performed in the northern basin (position ZG3; Figure 1). The current speed at the deepest location was slightly lower than that measured at the mean depth.

a) The "Alpnachersee case": For a typical bottom current velocity $u_{1m} \approx 2.6$ cms^{-1} (as determined from Figure 2, see details below), (2) yields $L_{MO} > 100$ m (Figure 7), a length which is several times larger than the depth of the hypolimnion. Consequently, biogenic stratification cannot build up in such a system, since bottom-induced mixing overcomes the stratifying effect of the dissolved solids.

b) The "Zugersee case": During the winter period under consideration, $u_{1m} \approx 1.7$ cms^{-1} (as determined from Figure 6a, see details below), and (2) yields $L_{MO} \approx 35$ m (Figure 7). The fact that L_{MO} is indeed much smaller than the thickness of the permanently stratified deep-water body, which typically extends from about 80 m down to the lake bottom (Figure 5a), is consistent with the long-term stability of the water mass. It means that deep bottom currents are not energetic enough to erode the permanent biogenic stratification over a long period of time. Indeed, an extreme storm event in 1982 was able to homogenize the deep water body – beginning at maximum depth – only minimally (Imboden et al., 1988).

The Monin-Obukhov argument explains the difference in large-scale vertical structure in the deep water between the two lakes, but not the difference in near-sediment density gradient. In order to understand why the internal seiche-induced bottom currents in Alpnachersee are apparently capable of redistributing the released ions, whereas in Zugersee the dissolved solids become accumulated above the sediment surface, we use another energy criterion. Laboratory experiments with density-stratified water have shown that the dissipation of turbulent kinetic energy has to fulfil the condition

$$\varepsilon > (15 \text{ to } 25) \cdot \nu N^2 \approx 20\, \nu N^2 \qquad [\text{Wkg}^{-1}] \qquad (3)$$

(Stillinger et al., 1983; Rohr et al., 1987) to produce "active" turbulence; i.e. irreversible diapycnal mixing with a non-vanishing buoyancy flux J_b (= $K_d N^2 > 0$). Equation (3) expresses the fact that for irreversible diapycnal mixing to occur (diffusivity $K_d > 0$), the turbulent eddies have to overcome the suppressing effects of viscosity ν and stability N^2.

In Figure 7, the energy criterion of (3) has been applied to the near-sediment stability N^2 of the two situations discussed above (Figures 4a and 5b); i.e. to $N^2 \approx 7 \cdot 10^{-7} s^{-2}$ (Alpnachersee) and $N^2 \approx 8 \cdot 10^{-3}\ s^{-2}$ (Zugersee). The corresponding turbulence levels $20\nu N^2$ (Alpnachersee: $\approx 2 \cdot 10^{-11}$ Wkg^{-1}; Zugersee: $\approx 2 \cdot 10^{-7}$ Wkg^{-1}) are compared to the turbulent dissipation of a steady, logarithmic boundary layer, as described by (1). It turns out that in the case of Alpnachersee, even for small currents of 1 cms^{-1}, $\varepsilon = u_*^3/(kz)$ overcomes the critical activity level $20\nu N^2$ at a distance from the sediment as great as the maximum thickness $\delta_{mix} \approx 4$ m (Figure 7). However, in the case of Zugersee, a current of 3 cms^{-1} (which we regard as a long-term maximum in the deepest part of this lake) would not be

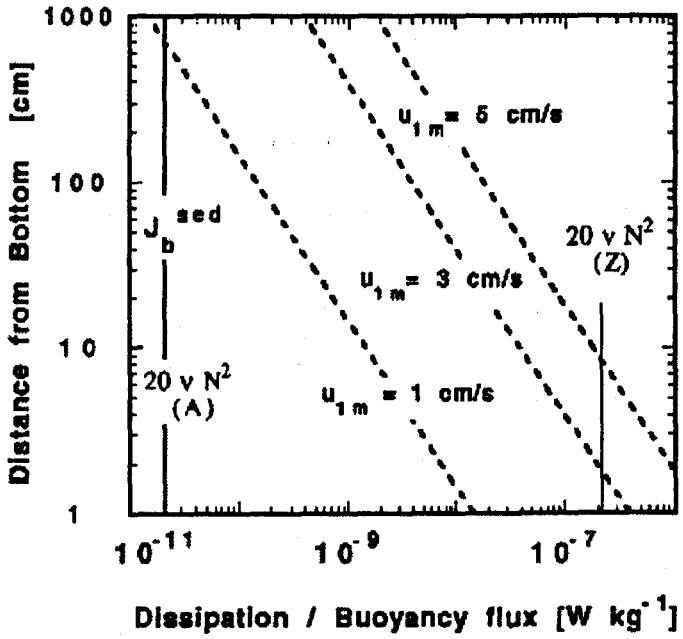

Figure 7. Rates of dissipation of turbulent kinetic energy calculated by similarity scaling (drag coefficient $C_{1m} = 1.6 \cdot 10^{-3}$) as a function of distance from the sediment, and as a function of the bottom current velocity u_{1m} (dashed lines), are compared to: (1) $J_b^{sed} \approx 2 \cdot 10^{-11}$ Wkg^{-1}, the buoyancy flux due to the release of dissolved solids (black line, left), and (2) $20\nu N^2$ (thin lines), the criterion for active turbulence in stratified water, applied to the near-sediment stratification of Alpnachersee (A) and Zugersee (Z) (20 cm thick suppression layer) (note: J_b^{sed} coincides with $20\nu N^2$ in Alpnachersee). Monin-Obukhov lengths L_{MO}, the intersections of the lines of J_b^{sed} and ε, lay beyond the upper boundary of the figure (see text).

able to mix more than a layer of 2 cm above the sediment (Figure 7). As this scale is equal to the thickness δ_v of the viscous sublayer of a non-stratified fluid, given by $\delta_v = 10\nu/u_*$ (Hinze, 1975), we conclude that turbulence is suppressed in the 20 cm thick stratified near-sediment layer of Figure 5b. Consequently, the exchange within this layer is not turbulent, but drops progressively to the molecular level and thereby sustains the accumulation of dissolved solids. In the following, we will call this zone the "suppression" layer, the thickness of which will be denoted by δ_{sup}.

As an effect of suppressed turbulence and high density stratification above the sediment, the vertical exchange in the deepest part of Zugersee is expected to decrease. Indeed, analysis of the temperature profiles in Zugersee for a six-month winter period in 1992-93 (Müller, 1993) reveals a decrease in the diapycnal diffusivity K_d towards the sediment at the deepest part of the lake. In contrast, in Alpnachersee K_d is increasing in that zone. This difference will be discussed in the following two sections.

The Effectiveness of Bottom Boundary Mixing

In this section we evaluate the effect of the near-sediment stratification on the basin-wide (total bulk) diapycnal diffusivity in the deep-water body. The idea of expressing the basin-wide diapycnal diffusivity as a function of the mixing rate at the sediment boundary is not new, since Munk (1966) has already suggested that much of the ocean mixing might take place at the sloping boundary. Based on the observation of signatures of well-mixed layers advected away from sloping ocean bottom boundaries, Armi (1978, 1979) suggested estimating the basin-wide oceanic vertical diffusivity K_d by distinguishing between an interior diffusivity, K_d^I, and a boundary layer diffusivity, K_d^B. He proposed scaling the near-sediment diffusivity K_d^B, determined by the Rn-222 method (Broecker et al., 1968; Sarmiento et al., 1976; Chung and Kim, 1980), by the aspect ratio $\partial A(z)/\partial z \cdot \delta_{mix}(z) \cdot A^{-1}(z)$, which expresses the ratio of the ocean sediment surface of the mixed bottom layer $A_{sed}(z) = \partial A(z)/\partial z \cdot \delta_{mix}(z)$ at depth z (Figure 8) to the ocean cross-sectional area A(z):

$$K_d(z) = K_d^I(z) + K_d^B(z) \cdot \left\{ \partial A(z) / \partial z \cdot \delta_{mix}(z) \cdot A^{-1}(z) \right\} \qquad [m^2 s^{-1}] \qquad (4)$$

Garrett (1979, 1990) questioned the correctness of this formulation, since mixing of already well-mixed water near the sediment is less efficient. Instead, he proposed first determining the area-averaged buoyancy flux $J_b^{tot}(z)$ at depth z (Figure 8) and then calculating the diapycnal diffusivity

$$K_d(z) = J_b^{tot}(z) \cdot N^{-2}(z) \qquad [m^2 s^{-1}] \qquad (5)$$

by using the background (interior) stratification $N^2(z)$. A different approach was made, following Phillips' (1970) solution, to express the diapycnal diffusivity K_d as a function of the thickness δ_{mix} of the mixed bottom layer and the diffusivity K_d^B within that layer. Garrett (1990) showed that the total buoyancy flux $J_b^{tot}(z)$ is reduced by an effectiveness factor (defined below), which takes into account the fact that the stratification is not maintained all the way to the sediment. As this effectiveness factor is strongly dependent on K_d^B, which is difficult to determine experimentally, alternative models have to be considered. Imberger and Ivey (1993) extended Phillips' (1970) solution, valid for a sloping boundary, to a horizontal sediment bottom, and found a dependence of $K_d \sim \delta_{mix}^9$.

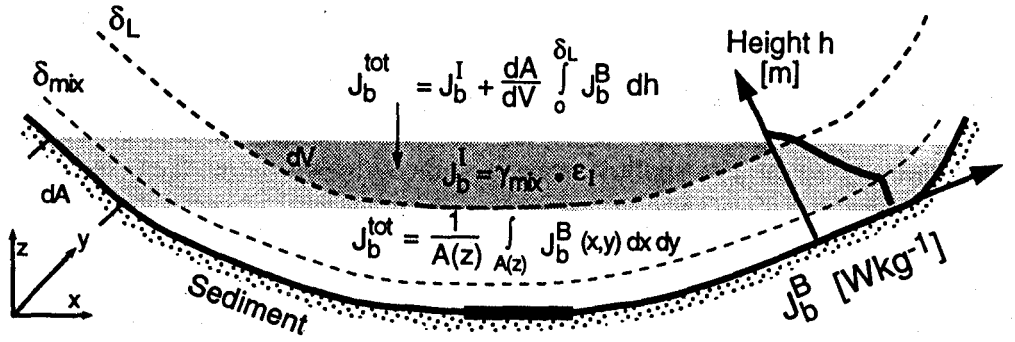

Figure 8. Schematic illustration of the boundary-layer model describing the total buoyancy flux J_b^{tot} as a function of the buoyancy fluxes J_b^I and J_b^B from the interior and from the bottom boundary, respectively. δ_L and δ_{mix} denote the thicknesses of the logarithmic and the well-mixed layer, respectively. h is the local height above the sediment. $\partial A/\partial V$ describes the sediment surface per unit volume of lake water as a function of depth.

This relation is of limited applicability, as the uncertainties in δ_{mix} present in spatially and temporally complex natural systems (Figure 4b), are amplified dramatically (e.g. a shift of 30% in δ_{mix} would lead to a change of K_d of an order of magnitude).

Faced with this unsatisfactory situation, we evaluate another boundary mixing model that is less sensitive to K_d^B and δ_{mix}. We follow Garrett's approach for the estimation of the total buoyancy flux $J_b^{tot}(z)$ at depth z by horizontally integrating the contributions from the interior $J_b^I(z)$ and the boundary $J_b^B(x,y,z)$, respectively, along the cross-sectional

$$J_b^{tot}(z) = J_b^I(z) + \frac{1}{A(z)}\int_{A(z)} J_b^B(x,y,z)\, dx\, dy \quad [Wkg^{-1}] \qquad (6)$$

area A(z), as depicted in Figure 8. Equation (6) is a simple balance for the potential energy and so far not specific to the model. The formulation of $J_b^B(x,y,z)$ is, however, dependent on the model and has to be specified. The basin-wide diapycnal diffusivity K_d is finally determined using (5).

To determine the buoyancy flux $J_b^B(x,y,z)$ in the boundary layer, we make the following model assumptions:

(a) The current in the bottom boundary follows a logarithmic profile up to a height δ_L, and the rate of dissipation is given by the scaling law $\varepsilon = u_*^3(kz)^{-1} = C_{1m}^{3/2} u_{1m}^3 (kz)^{-1}$. Water beyond δ_L is considered as interior water, with a dissipation rate ε_I defined by interior processes.

(b) The buoyancy flux J_b^B in the stratified part of the water column (interior or boundary layer) is a constant fraction γ_{mix} of the dissipation rate ε; i.e. $J_b^B = \gamma_{mix} \cdot \varepsilon$.

(c) Within the extremely stratified suppression layer of thickness δ_{sup}, $J_b^B = 0$, ($\gamma_{mix} = 0$).

(d) The heat flux between sediment and water is neglected. Consequently, the buoyancy flux J_b^B decreases linearly to zero within a well-mixed layer when approaching the sediment (as does the heat flux).

Assumption (a) is based on several experimental observations (e.g. Dewey and Crawford, 1988; Weatherly and Martin, 1978; Weatherly and Wimbush, 1980), and assumption (c) is motivated by profiles of the type shown in Figure 5b. The mixing efficiency γ_{mix}, required for assumption (b), is surely not a constant. However, since no practical parameterization is available, we use the constant $\gamma_{mix} = 0.12$ (Peters and Gregg,

1988), which lies well within the range of other estimates (Osborn, 1980; Ivey and Imberger, 1991). In addition this choice is justified by the finding that γ_{mix} does not depend on the level of turbulence (Peters and Gregg, 1988). Assumption (d) has to be tested separately for each individual water basin (it is well fulfilled for Alpnachersee as the heat flux within the relatively shallow water column is much larger than sediment-water heat exchange).

The weak point among assumptions (a) to (d) is the poorly defined choice of the thickness of the logarithmic layer, which, based on experiment (Wüest et al., 1996a), has been chosen as $\delta_L = 10$ m. However, changes in δ_L by a factor of 2 modify the dissipation, and therefore the buoyancy flux $J_b^{tot}(z)$ (6), integrated over the logarithmic layer, by only 10%, as can easily be calculated from (7). Given all the uncertainties in the available data and the inhomogeneities of such natural basins, we consider this deficiency to be acceptable.

Based on the above assumptions (a) to (d), on the constants γ_{mix}, δ_L and $C_{1m} = 1.6 \cdot 10^{-3}$ (smooth bottom, Elliott, 1984), and on a specified topography, we are now able to determine the horizontally-averaged buoyancy flux $J_b^{tot}(z)$ from a given horizontal velocity field $u_{1m}(x,y,z)$ as a function of depth z using (6). In order to integrate (6), it is helpful to distinguish between (1) different distances from the maximum lake depth and (2) three different types of stratification.

Close to the maximum depth of the lake, the total buoyancy flux of (6) is made up entirely of contributions from within the logarithmic layer (Figure 8, lower layer). It is therefore not possible to simplify (6), and the integration has to be carried out by an appropriate procedure over the entire cross-sectional area A(z).

If, on the other hand, the vertical distance between z and the maximum depth is larger than the thickness δ_L of the logarithmic layer, (6) is simplified considerably. The horizontal area within the bottom boundary can be approximated by the sediment surface within the layer being considered (i.e. $dA \cdot A^{-1} = \partial A/\partial V \cdot dz$). In addition, the horizontal integration can be replaced by vertical integration over the thickness δ_L, as shown schematically in Figure 8. Consequently, the total buoyancy flux is then calculated by

$$J_b^{tot}(z) = J_b^I(z) + \frac{\partial A}{\partial V}(z) \int_0^{\delta_L} J_b^B(h,z)\, dh \qquad [Wkg^{-1}] \qquad (7)$$

where h is the vertical co-ordinate originating at the local lake bottom (Figure 8).

For a bottom boundary layer stratified all the way to the sediment (i.e. to the viscous sublayer $\delta_V = 10\nu/u_*$), integration of (7) (neglecting small terms proportional to the sine of the bottom slope) yields

$$J_b^{tot}(z) = \gamma_{mix} \cdot \left[\varepsilon_I(z) + \frac{\partial A}{\partial V}(z) \frac{u_*^3}{k} \ln\left(\frac{\delta_L}{\delta_V}\right) \right] \quad [Wkg^{-1}] \qquad (7a)$$

where $J_b^B(h)$ has been replaced by $\gamma_{mix} \cdot \varepsilon(h)$ and $\varepsilon(h)$ by $u_*^3\,(kh)^{-1}$ (the dependence of u_*^3 and δ_L on depth z is not indicated). If the bottom boundary layer consists of a stratified and a well-mixed layer of thicknesses $\delta_L - \delta_{mix}$ and δ_{mix}, respectively, as observed in Alpnachersee (Figure 4a), then integration of (7) leads to

$$J_b^{tot}(z) = \gamma_{mix} \cdot \left[\varepsilon_I(z) + \frac{\partial A}{\partial V}(z) \left\{ \int_0^{\delta_{mix}} J_b^B(h,z)\, dh + \int_{\delta_{mix}}^{\delta_L} J_b^B(h,z)\, dh \right\} \right]$$

$$= \gamma_{mix} \cdot \left[\varepsilon_I(z) + \frac{\partial A}{\partial V}(z) \left\{ \frac{\delta_{mix}}{2} J_b^B(\delta_{mix}) + \frac{u_*^3}{k} \ln \left(\frac{\delta_L}{\delta_{mix}} \right) \right\} \right]$$

$$= \gamma_{mix} \cdot \left[\varepsilon_I(z) + \frac{\partial A}{\partial V}(z) \frac{u_*^3}{k} \left\{ \frac{1}{2} + \ln \left(\frac{\delta_L}{\delta_{mix}} \right) \right\} \right] \quad [Wkg^{-1}] \quad (7b)$$

In cases such as Zugersee, where the bottom boundary layer is made up of a stratified layer and a suppression layer (Figure 5b), integration of (7) yields

$$J_b^{tot}(z) = \gamma_{mix} \left[\varepsilon_I(z) + \frac{\partial A}{\partial V}(z) \frac{u_*^3}{k} \ln \left(\frac{\delta_L}{\delta_{sup}} \right) \right] \quad [Wkg^{-1}] \quad (7c)$$

In order to make equation (7a,b,c) easier to interpret, we show in Figure 9a the vertical structure of the buoyancy fluxes $J_b^B(h)$ for the three cases discussed. Whereas $J_b^B(h)$ increases toward the sediment in the stratified case, $J_b^B(h)$ decreases linearly within the well-mixed layer and drops to zero within the suppression layer.

The effect of both the mixed and the suppression layers is to lead to a reduction in the effectiveness of boundary mixing with increasing thicknesses δ_{mix} and δ_{sup}, respectively, of the layers. We define effectiveness identically to Garrett (1990) as the ratio $J_b^{tot\text{-}mix}$, the total buoyancy flux including a well-mixed layer, to $J_b^{tot\text{-}strat}$, the total buoyancy flux that would occur if there were stratification all the way down to the sediment. Figure 9b shows quantitatively the effect of the well-mixed layer thickness δ_{mix} to the effectiveness of boundary mixing. For very thin well-mixed layers ($\delta_{mix} \rightarrow \delta_V$), the effectiveness is 1 by definition. It decreases to about 7% in the other extreme case, when the whole logarithmic layer is mixed ($\delta_{mix} \rightarrow \delta_L$).

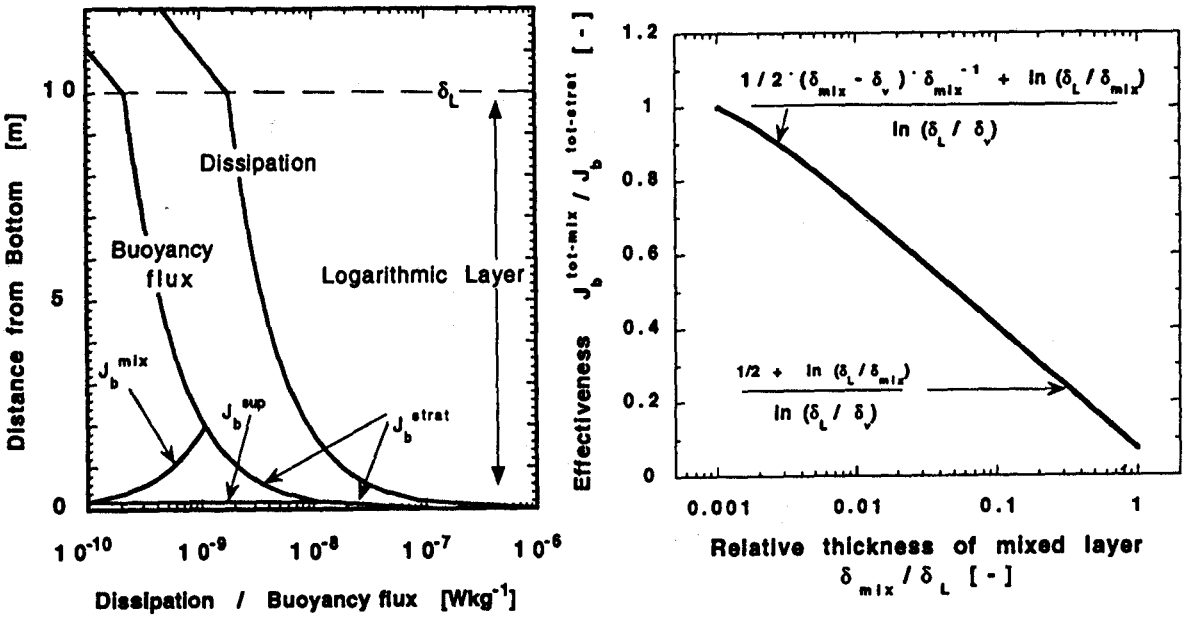

Figure 9. (a) Buoyancy flux as a function of height above the sediment within the logarithmic layer for three cases, *viz.* "stratified", "well-mixed" and "suppression" layers. The break-off to interior values at δ_L is drawn arbitrarily. Figure 9. (b) Effectiveness (definition in text) as a function of the relative thickness δ_{mix}/δ_L of the mixed layer (here we have set $\delta_L = 10$ m and $\delta_V = 1$ cm, but these values are not critical).

Application of the Boundary Mixing Model

In this section, the model predictions (Equations 5 and 6) are compared to observations from Alpnachersee and Zugersee. Since these two lakes have relatively simple basin shapes (Figure 1), but are very different in terms of stratification, external forcing and mixing, we consider them as ideal candidates to test the model. As detailed information on the horizontal flow field u_{1m} (x,y,z) is missing, we simplify the problem by using the two near-bottom current records $u_{1m}(t)$ shown in Figures 2 and 6. We consider this simplification to be appropriate in the deep hypolimnion of morphologically simple basins, as long as bottom currents are dominated by first horizontal internal seiche modes (Münnich, 1993). In addition, we assume for both lakes that internal mixing can be neglected in the deep hypolimnion and therefore set $\varepsilon_I = 0$. This approximation is appropriate, as it has been shown for Alpnachersee by tracer experiments (Goudsmit et al., 1996) and by microstructure measurements (Wüest et al., 1996a) that mixing in the interior is an order of magnitude weaker than the horizontal basin average. This is even more pronounced in the very deep part, where $\partial A/\partial V$ is large.

a) *Alpnachersee*: As input to the model we use the current data shown in Figure 2, which were collected 1.4 m above the sediment at the deepest part of the lake (Figure 1) during a period of 56 days in June-July 1994. From this record, a mean value for u_{1m}^3 of $(2.6 \text{ cm s}^{-1})^3$ was determined, which is used in (1), (6) and (7). The lower part of the bottom boundary in Alpnachersee is a well-mixed layer, with a thickness δ_{mix} of 4 to 5 m near maximum depth (Figure 4a). Upslope, the thickness is continuously decreasing (Figure 4b).

The total buoyancy flux $J_b^{tot}(z)$ is calculated using (6) and (7b), integrating over the entire cross-sectional area A(z) in vertical steps of 20 cm, and using the lake-specific topographic function $\partial A/\partial V(z)$ and the thickness $\delta_{mix}(z)$. The diapycnal diffusivity $K_d(z)$ is finally determined by applying (5) and using a representative water column stability $N^2(z)$ for the period during June-July 1994.

Within the deepest 10 m of the lake, the diapycnal diffusivity in Alpnachersee (Figure 10a) shows two main features. The diffusivity is (1) low due to the overall strong stratification N^2 and (2) increasing towards the sediment, since the stability N^2 is extremely low in the well-mixed bottom layer. The comparison between model results and long-term basin-wide diffusivities determined by the heat-budget method (Powell and Jassby, 1974) is also shown in Figure 10a. It turns out that both (1) the absolute value and (2) the vertical shape of $K_d(z)$ are in excellent agreement without having to tune any of the model parameters. Nevertheless, the agreement in the vertical structure of $K_d(z)$ is partly accidental, since the heat-budget method has a relatively large error within 4 m of maximum depth. The uncertainty is due to (1) the unknown sediment-water heat flux (the lake is not meromictic like Zugersee) and (2) the poorly defined vertical gradients in the "well-mixed" bottom layer. This second deficiency may be especially misleading when vertical gradients close to the deepest point in the lake are determined by averaging CTD or thermistor profiles in vertical (Eulerian) bins and thereby - due to the seiching motion - averaging over both well-mixed and stratified water layers.

b) Zugersee: In applying the model to Zugersee we follow the same procedure as above. As input we use the current data shown in Figure 6, which were measured at 1.8 m above the sediment at the deepest point in the lake in February 1993 (during 37 days). Averaging the third power of the bottom current u_{1m} leads to a value of $(u_{1m})^3 = (1.7 \text{ cms}^{-1})^3$, which is again introduced into (1), (6) and (7). Since the hypolimnetic water column is stratified all the way down to the sediment, as shown in Figure 5a, the stratified bottom

boundary case is applicable. Consequently, the total buoyancy flux is determined by (7a) again using the topographic function $\partial A/\partial V(z)$. Finally, the diapycnal diffusivity $K_d(z)$ was calculated using (5) with the stability $N^2(z)$ determined from CTD profiles taken in March 1993.

The result for $K_d(z)$ is shown in Figure 10b, where it is also compared to the values determined by the heat-budget method for a six-month period during winter 1992-1993. Again, it turns out that both (1) the absolute value and (2) the approximate vertical shape of $K_d(z)$ are in good agreement without tuning any of the model parameters. Near maximum depth, the model apparently slightly overestimates the diffusivity. Besides the experimental uncertainties, this disagreement is most probably due to the suppression layer. Given the observed thickness of the suppression layer of about 20 cm (Figure 5b), application of (7c) would indeed reduce the model diffusivity by the factor $\ln(\delta_L/\delta_v)$ / $\ln(\delta_L/\delta_{sup}) \approx 1.8$ (arrow in Figure 10b). Since the lateral structure of the suppression layer is not known, this correction is not defined well enough to be included in Figure 10b. Even though the good agreement may to some extent be accidental, the decrease in the diapycnal diffusivity towards the sediment at maximum depth is consistent with the model.

Although one should be cautious not to overinterpret the agreement between model and data (there are numerous possible sources of deviations: e.g. varying drag coefficients, irregular topography, etc.), we can conclude that the model is excellently consistent with the absolute values as well as with the vertical profile of diapycnal diffusivity, both of

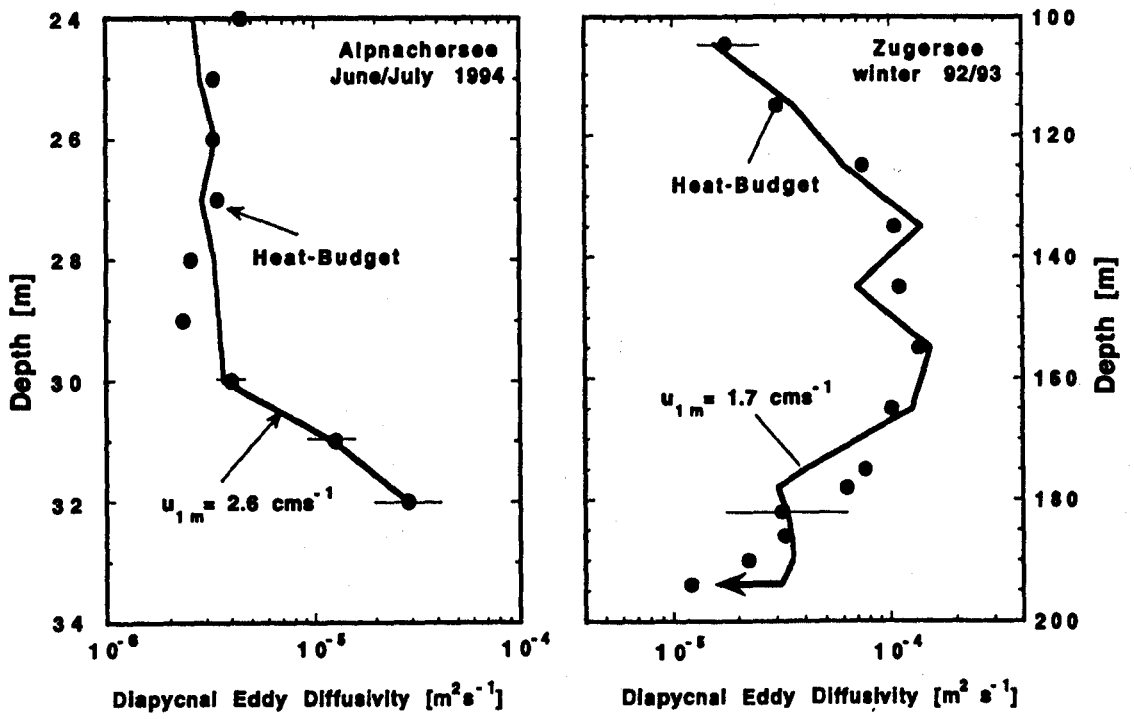

Figure 10. Comparison of diapycnal diffusivity K_d in Alpnachersee (a) and Zugersee (b), determined by the heat budget method (black dots), with the boundary mixing model (line, Equations 5 and 6; see text). The heat budget was applied over periods of 6 months in Zugersee (winter 92/93) and 2 months in Alpnachersee (June/July 94) (note the different vertical scales). The value of 1.1 cm^2 s^{-1} obtained for K_d in the weakly stratified part of the hypolimnion of Zugersee ($\approx$ 120 to 160 m depth) is supported by the long-term oxygen balance of the deep water (Wehrli et al., 1994). The effect of the suppression of turbulence (within a 20-cm inactive bottom layer) on the model result is shown by the arrow (factor 1.8). Data from Gloor (1995) and Müller (1993) for Alpnachersee and Zugersee, respectively.

which are caused by boundary mixing alone. Interestingly, near maximum depth the K_d's of the two lakes have about the same value, even though the mechanisms are very different: weak but efficient mixing in one case (Zugersee), strong and inefficient in the other case (Alpnachersee).

Conclusions

Based on experimental observations, theoretical considerations and modelling, an analysis of diapycnal (vertical) mixing was conducted in the deep water of two lakes exhibiting significantly different characteristics of density stratification and external forcing. The following conclusions can be drawn:

(1) The degree of stratification of the deep-water column is not only the result of external physical forcing at the surface, but also of the rate of release of dissolved solids from the sediment. The latter is determined mainly by long-term photosynthetic productivity in the epilimnion.

(2) For lacustrine systems with low kinetic energy input over periods of weeks, the accumulation of dissolved solids above the sediment-water interface leads to the formation of a highly stratified layer. Within this layer turbulence is almost completely suppressed and diffusion drops to molecular levels. Consequently, the basin-wide diapycnal diffusivity decreases with increasing thickness of the suppression layer.

(3) Aquatic systems with high kinetic energy input - relative to the buoyancy flux due to the release of dissolved solids - reveal well-mixed layers near the sediment.

(4) The most relevant parameters governing the two different regimes are the bottom current speed and the rate of release of dissolved solids from the sediment. The ratio of boundary-induced mixing to the flux of ions from the sediment determines whether the near-sediment layer is highly stratified or well-mixed.

(5) The presence of such well-mixed or highly stratified near-sediment layers reduces the effectiveness of boundary mixing and diminishes the basin-wide buoyancy flux as well as the diapycnal diffusivity.

(6) With a simple boundary mixing model, assuming (a) smooth flow in a logarithmic boundary layer of constant thickness, where the rate of turbulent dissipation follows the scaling law (Eq. 1), (b) constant mixing efficiency γ_{mix} in the stratified water column, and (c) no heat flux through the sediment, we have been able to quantify the basin-wide rate of diapycnal mixing. Application of the model to two lakes in which both density stratification and external forcing differ significantly reproduced astonishingly well the absolute values as well as the vertical structure of the diapycnal diffusivity in the deep hypolimnion.

(7) The presented model is consistent with tracer observations in medium-sized lakes (Goudsmit et al., 1996), demonstrating that diapycnal mixing in the deep water is driven entirely by boundary mixing. Application of the model to other systems in which horizontal current structure is better defined will hopefully show the model to have a wide range of applicability.

Acknowledgments. We are indebted to many members of the Environmental Physics Department at EAWAG, too numerous to mention, for making the collection of field data possible; our special thanks, however, go to M. Schurter for his unfailing presence on the lakes during the entire sampling program. Figure 5b was kindly provided by B. Wehrli. Part of the drawing and typing work was done by H. Bolliger and V. Graf, respectively.

The constructive criticism of two anonymous reviewers helped to improve the manuscript. D. M. Livingstone "styled" the English. This study was supported by Swiss National Science Foundation grants 20-32700.91 and 20-36364.92.

References

Armi, L., Some evidence for boundary mixing in the deep ocean, *J. Geophys. Res., 83*, 1971-1979, 1978.

Armi, L., Effects of variation in eddy diffusivity on property distributions in the ocean, *J. Mar. Res.*, 37, 515-530, 1979.

Brandl, H., and K. Hanselmann, Evaluation and application of dialysis porewater samplers for microbiological studies at sediment-water interfaces, *Aquat. Sci., 53*, 55-73, 1991.

Broecker, W. S., J. Cromwell, and Y. H. Li, Rates of vertical eddy diffusion near the ocean floor based on measurements of the distribution of excess Rn-222, *Earth Planet. Sc. Lett.*, 5, 101-105, 1968.

Chen, C. T., and F. J. Millero, Precise thermodynamic properties for natural waters covering only the limnological range, *Limnol. Oceanogr.*, 31, 657-662, 1986.

Chung, Y., and K. Kim, Excess Rn-222 and the benthic boundary layer in the western and southern indian ocean, *Earth Planet. Sc. Lett.*, 49, 351-359, 1980.

Dewey, R. K., and W. R. Crawford, Bottom stress estimates from vertical dissipation rate profiles on the continental shelf, *J. Phys. Oceanogr., 18*, 1167-1177, 1988.

Elliott, A. J., Measurements of the turbulence in an abyssal boundary layer, *J. Phys. Oceanogr., 14*, 1779-1786, 1984.

Finckh, P., Heat-flow measurements in 17 perialpine lakes: Summary, *Geological Soc. Am. Bull*, Part I, 92, 108-111, 1981.

Garrett C., Mixing in the ocean interior, *Dyn. Atmos. Oceans, 3*, 239-265, 1979.

Garrett, C., The role of secondary circulation in boundary mixing, *J. Geophys. Res., 95*, 3181-3188, 1990.

Garrett, C., Marginal mixing theories, *Atmosphere Ocean, 29*, 313-339, 1991.

Gloor, M., A. Wüest, and M. Münnich, Benthic boundary mixing and resuspension induced by internal seiches, *Hydrobiologia, 284*, 59-68, 1994.

Gloor M., Methode der Temperaturmikrostruktur und deren Anwendung auf die Bodengrenzschicht in geschichteten Wasserkörpern, *Dissertation ETH Zürich*, Nr. 11'336, p. 159, 1995.

Goudsmit, G. H., F. Peeters, M. Gloor and A. Wüest, Boundary versus internal diapycnal mixing in stratified waters, 1996, *J. Geophys. Res. 102*, 27903-27914, 1997.

Hinze, J. O., *Turbulence*, McGraw-Hill, New York, 618 pp., 1975.

Imberger, J., and G. N. Ivey, Boundary mixing in stratified reservoirs, *J. Fluid Mech., 248*, 477-491, 1993.

Imberger, J., and J. C. Patterson, Physical limnology, in *Advances in applied mechanics*, edited by J. W. Hutchinson and T. Y. Wu, Academic Press, Cambridge, 303-475, 1990.

Imboden, D. M., B. Stotz and A. Wüest, Hypolimnic mixing in a deep alpine lake and the role of a storm event, *Verh. Internat. Verein, Limnol., 23*, 67-73, 1988.

Imboden, D. M., and A. Wüest, Mixing mechanisms in lakes, p. 83-138, In *Lakes: Chemistry, Geology, Physics*, edited by A. Lerman, D. M. Imboden and J. Gat, Springer, New York, 1995.

Ivey, G. N., The role of boundary mixing in the deep ocean, *J. Geophys. Res., 92*, 11'873-11'878, 1987.

Ivey, G. N., and J. Imberger, On the nature of turbulence in a stratified fluid. Part I: The energetics of mixing, *J. Phys. Oceanogr., 21*, 650-659, 1991.

Müller, B., Sauerstoffentwicklung im Zugersee, *Diplomarbeit EAWAG/ETH*, 1993.

Münnich, M., A. Wüest, and D. M. Imboden, Observations of the second vertical mode of the internal seiche in an alpine lake, *Limnol. Oceanogr.*, 37, 1705-1719, 1992.

Münnich, M., On the influence of bottom topography on the vertical structure of internal seiches, *Dissertation EAWAG/ETH Zürich*, Nr. 10434, 1993.

Munk, W. H., Abyssal recipes, *Deep-Sea Res., 13*, 707-730, 1966.

Osborn, T. R., Estimates of the local rate of vertical diffusion from dissipation measurements, *J. Phys. Oceanogr. 10*, 83-89, 1980.

Peters, H., and M. C. Gregg, Some dynamical and statistical properties of equatorial turbulence, In *Small-scale Turbulence and Mixing in the Ocean, Proc. 19th Intnl Liège Colloquium on Ocean Hydrodynamics*, edited by J. C. J. Nihoul and B. M. Jamart, Elsevier, Amsterdam, 185-200, 1988.

Phillips, O. M., J. H. Shyu, and H. Salmun, Experiment on boundary mixing: mean circulation and

transport rates, *J. Fluid Mech., 17*, 473-499, 1986.
Phillips, O. M., On flows induced by diffusion in a stably stratified fluid, *Deep-Sea Res., 17*, 435-443, 1970.
Powell, T., and A. Jassby, The estimation of vertical eddy diffusivities below the thermocline in lakes, *Water Resour. Res., 10*, 191-198, 1974.
Press, W. H., B. P. Flannery, S. A. Teukolsky, and W. T. Vetterling, Numerical recipes, Cambridge University Press, Cambridge, 1986.
Rohr, J. J., K. N. Helland, E. C. Itsweire, and C. W. Van Atta, Turbulence in a stably stratified shear flow: A progress report, In *Turbulent Shear Flows 5*, Springer-Verlag, Berlin, 1987.
Sarmiento, J. L., H. W. Freely, W. S. Moore, A. E. Bainbridge, and W. S. Broecker, The relationship between vertical eddy diffusion and buoyancy gradient in the deep sea, *Earth Planet. Sci. Lett., 32*, 357-370, 1976.
Stillinger, D. C., K. N. Helland, and C. W. Van Atta, Experiments on the transition of homogeneous turbulence to internal waves in a stratified fluid, *J. Fluid Mech., 131*, 91-122, 1983.
Thorpe, S. A., The dynamics of the boundary layers of the deep ocean, *Sci. Prog., Oxford, 72*, 189-206, 1988.
Toole, J. M., K. L. Polzin, and R. W. Schmitt, Estimates of diapycnal mixing in the abyssal ocean, *Science, 264*, 1120-1123, 1994.
Weatherly, G. L., and P. J. Martin, On the structure and dynamics of the oceanic bottom boundary layer, *J. Phys. Oceanogr., 8*, 557-570, 1978.
Weatherly, G. L., and W. Wimbush, Near-bottom speed and temperature observations on the Blake-Bahama outer ridge, *J. Geophys. Res., 85*, 3971-3981, 1980.
Wehrli, B., A. Wüest, and D. M. Imboden, Grundlagen für die Sanierung des Zugersees: Untersuchungen des Stoffhaushaltes von Tiefenwasser und Sediment, EAWAG, Dübendorf, Auftrag 37-4840, 1994.
Wehrli, B., A. Wüest, and D. M. Imboden, Sind biogen meromiktische Seen intern sanierbar? Fallbeispiel Zugersee, in *Limnologie Aktuell*, edited by D. Jaeger and R. Koschel, *8*, 29-37, 1995.
Wüest, A., D. C. van Senden, J. Imberger, G. Piepke, and M. Gloor, Comparison of diapycnal diffusivity measured by tracer and microstructure techniques, *Dyn. Atmos. Oceans 24*, 27-39, 1996a
Wüest, A., G. Piepke and J. D. Halfman, Combined effects of dissolved solids and temperature on the density stratification of Lake Malawi (East Africa), In *The Limnology, Climatology and Paleoclimatology of the East African Lakes*, edited by Johnson, Gordon and Breach Scientific Publishers, NY, p. 183-202, 1996b.
Wunsch, C., On oceanic boundary mixing, *Deep-Sea Res., 17*, 293-301, 1970.